



EYE-CLIMA

Verifying emissions
of climate forcers

Inventory of point source emissions of CH₄ estimated from high- resolution satellite data

DELIVERABLE 1.4

Author(s): Hartmut Bösch, Michael Hilker
Date of submission: 11-03-2025
Version: 1.0
Responsible partner: University of Bremen
Deliverable due date: 31-12-2024
Dissemination level: Public

Call: HORIZON-CL5-2022-D1-02
Topic: Climate Sciences and Responses
Project Type: Research and Innovation Action
Lead Beneficiary: NILU - Norsk Institutt for Luftforskning



Document History

Version	Date	Comment	Modifications made by
0.1	07-03-2025	First Draft	Michael Hilker, Hartmut Bösch (University of Bremen)
0.2	07-03-2025	Internal review	Rona Thompson (NILU)
1.0	11-03-2025	Submitted to Commission	Rona Thompson (NILU)



Summary

The aim of this deliverable is to first provide an overview over the retrieval methods applied to high-resolution, hyperspectral instruments for methane enhancements and to apply those methods to the multispectral imagers PRISMA, EnMAP and EMIT to evaluate methane point source emissions over Europe. We have identified 14 different potential locations (some have multiple emission points) and we have inferred methane enhancements for all available, cloud-free satellite measurements. Using a number of criteria, we have classified each satellite scene if a plume can be identified and if an emission rate can be reliably estimated. Emissions have been estimated for 5 landfills, 2 unknown targets and 6 coal mining ventilation shafts with emission values ranging from 0.35 ± 0.37 t/h to 6.82 ± 2.13 t/h. With the exception of landfills near Thessaloniki and Bucharest, only a single scene is available for each different target so that our estimates represent only instantaneous emissions. The estimated emissions have been compared against values from bottom-up inventory E-PRTR and from the Polish State Mining Authority (WUG), and where available, against estimates from the Carbon Mapper portal and GHGSat values taken from the literature.



TABLE OF CONTENTS

Document History.....	2
Summary	3
1. Introduction	5
2. Deviations from Description of Work	6
3. Technical & Scientific progress / Methodology	7
3.1 Forward Modelling and Methane Enhancement Retrieval from Hyperspectral Satellite Observations.....	7
3.2 Emissions Estimation Using the Cross-Sectional-Flux (CSF) Method	8
3.3 Used Datasets	10
3.4 Target Selection.....	10
3.5 Data Processing	12
4. Results & Discussion.....	13
4.1 Comparison of three Retrieval Methods.....	13
4.2 Comparison of CH ₄ enhancement retrievals from the three satellite missions	14
4.3 Plume Scoring	15
4.4 Plume results	16
4.5 Comparisons of HiFi (EMIT) with Carbon Mapper (EMIT)	20
4.6 Estimation of Emissions	22
5. Conclusion and outlook	28
6. Acknowledgement	28
7. References	30
8. Appendix.....	32



1. Introduction

Measurements from hyperspectral and multispectral satellite imagers with spectral bands in the short-wave-infrared spectral region allow the retrieval of atmospheric methane anomalies with high spatial resolution of tens of meters. Although such satellite observations provide only sparse coverage, they allow methane emission values to be estimated on a facility-level at the time of overpass. Thus, observations from these high-resolution satellites complement measurements from satellite sensors like TROPOMI that provide us with daily global coverage but with a low spatial resolution of 7km.

Hyperspectral and multispectral satellite instruments have not been designed for spectral retrievals of trace gases and their measurements are carried out with comparably low spectral resolution. The applied retrieval methods are different to those used for sensors like TROPOMI and we will provide an overview over the retrieval methods for multispectral sensors including PRISMA, EnMAP and EMIT, that have been developed at IUP Bremen as part of the HiFi (High resolution Fit) software package. From the inferred atmospheric methane anomalies, methane emission plumes can be detected and the emission can be estimated using mass conservation methods.

We have carried out a survey of methane point sources over Europe using publicly available observations from the PRISMA, EnMAP and EMIT satellites. When a plume has been identified, the emission value has been estimated and assessed against values from bottom-up inventories E-PRTR and Polish State Mining Authority (WUG), and where available, against estimates from the Carbon Mapper portal and values from the literature.



2. Deviations from Description of Work

The low detection limit of hyperspectral sounders like Sentinel-2 of about 3 t/h is not well suited for the detection of CH₄ plumes for European locations. Multispectral sounders have better detection capabilities for detecting emission plumes for smaller emission sources. In addition to PRISMA, we have now also data from the multispectral sounders EnMAP and EMIT. EnMAP and EMIT have similar spectral characteristics to PRISMA but with higher signal-to-noise which increases the chances of successful plume detection. Thus, we have used EnMAP and EMIT in addition to PRISMA, instead of Sentinel-2.



3. Technical & Scientific progress / Methodology

3.1 Forward Modelling and Methane Enhancement Retrieval from Hyperspectral Satellite Observations

In hyperspectral satellite observations, the scene is represented as a grid of ground pixels, with each ground pixel having a corresponding measured spectrum. From each measured spectrum of a scene, we retrieve the methane enhancement by fitting a simulated spectrum to the observed spectrum y . To simulate a spectrum, we use a forward model F , which describes the relationship between the state vector x (the geophysical parameters of interest) and the measured spectral data. This relationship can be expressed as:

$$y = F(x) + \varepsilon$$

where ε represents measurement noise. The state vector x includes the free parameters of the model including the methane enhancement relative to the background. The forward model incorporates the effects of radiative transfer in the atmosphere, of the surface reflectance, and of the instrument. For simplicity, the instrument's influence is omitted in the following description.

To solve for x assuming a linear forward model around a linearization point x_0 , we use a linear least square fitting approach:

$$x = [K^T S_\varepsilon^{-1} K]^{-1} K^T S_\varepsilon^{-1} (y - F(x_0))$$

where S_ε is the covariance matrix associated with the measurement noise ε , and K is the Jacobian matrix of the forward model F evaluated at x_0 .

For a homogeneous scene where, spectral variations are primarily due to a small methane enhancement Δc in a small plume relative to the entire scene, the average scene spectrum \bar{y} and a perturbation Δc provide a sufficient forward model:

$$F(x) = \bar{y} + \frac{\partial F}{\partial c} \Delta c$$

3.1.1 Accounting for Scene Inhomogeneity

Real-world scenes are typically inhomogeneous, with surface reflectance varying from pixel to pixel. To address this inhomogeneity, we have implemented three different methods in HiFi, to enhance the forward model:

- **Matched Filter Approach (MF):** In this method, we assume that all deviations from the average scene spectrum \bar{y} follow a normal distribution. This allows us to use the simple forward model above, interpreting all deviations as forward model error within the noise term ε . The full covariance matrix S_ε is derived from the measured spectra of the scene. The Method is similar to (Thompson, et al., 2015).
- **Physics-based Forward Model (PhysicsF):** Here, we assume that the surface albedo is a polynomial function of wavelength λ , given by:

$$a(\lambda) = \sum_i^{N_{ply}} \alpha_i \lambda^i$$

This introduces N_{ply} additional coefficients α_i into the state vector x . The covariance matrix S_ε remains diagonal, reflecting measurement noise.

- **Principal Component Analysis (PCA):** When the plume occupies only a small fraction of the scene, its contribution to the overall spectral variability is minimal compared to other scene



effects. In this case, we apply Principal Component Analysis (PCA) to the spectra. The forward model is then constructed using a linear combination of the first N_{pca} principal components, which capture the most significant spectral variations. The state vector includes N_{pca} scaling factors for these components. The covariance matrix S_ϵ is again diagonal, reflecting the measurement noise. The Method is similar to (Joyce, et al., 2023).

3.1.2 Computation of the Jacobian Matrix

For our retrieval, we require the Jacobian Matrix K at the linearisation point x_0 . We select x_0 to represent the average state of the scene. We assume a non-scattering and absorption-only radiative transfer, which can be described using the Lambert-Beer law. This assumption allows us to compute analytic derivatives.

The absorption cross sections for methane (CH_4), water vapour (H_2O), and carbon dioxide (CO_2) are obtained from the HITRAN database. Temperature and pressure profiles, as well as the background concentrations for methane, H_2O , and CO_2 are obtained from ECMWF ERA5 (Hersbach, et al., 2017) data.

3.1.3 Handling Across-Track Variability

The measured scene exhibits additional variability due to slight differences in the detector's response for different across track pixels, as well as imperfect calibration. This variability often leads to stripping in the data, which is not fully addressed by the three methods described above. To account for this effect, we apply the methods individually to each across-track pixel, ensuring that the variability introduced by the detector response is appropriately handled.

3.2 Emissions Estimation Using the Cross-Sectional-Flux (CSF) Method

3.2.1 Description of the Method

Emissions are estimated from the retrieved methane enhancement maps using the Cross-Sectional-Flux (CSF) method. This approach is similar to those described in (Schneising, et al., 2020) (Schneising, et al., 2024) and (Fuentes Andrade, et al., 2024). The following steps are performed in sequence (and visualised in Figure 1):

1. The apparent plume source location and the plume direction are manually estimated from the methane enhancement maps
2. The data are resampled onto a new grid with a 5 m by 5 m sampling distance, aligned with the apparent plume direction.
3. Missing data are interpolated by calculating a weighted average for each missing ground pixel. The weight is based on an exponential function of the distance.
4. A rectangular subset of the data is selected, containing both plume and background pixels unaffected by the plume.
5. The average of the background pixels in the rectangular subset is subtracted from all pixels to remove large-scale variations.
6. The resampled data within the subset form equally spaced lines perpendicular to the plume direction. These lines are used as cross sections for flux calculation.
7. The flux q_i through each cross section i is computed as:

$$q_i = \sum_j \Delta c_{ij} L v$$



where Δc_{ij} is the methane enhancement (mass per unit area) in the j -th pixel of the i -th cross section, $L = 5m$ is the distance between adjacent pixels, and v is the average wind speed in the boundary layer.

8. The total emission rate Q is the average flux of all N_{CS} valid cross sections:

$$Q = \frac{1}{N_{CS}} \sum_i q_i$$

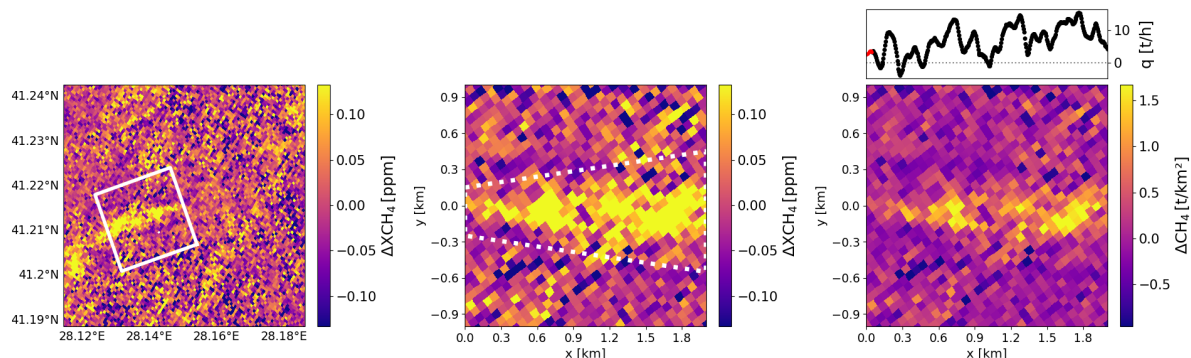


Figure 1: Left: Map showing retrieved methane enhancements, with the white box indicating the plume area. Centre: After rotation, sampling, and gap-filling, with the white dotted polygon representing the plume mask. Right: After background correction and unit conversion. Top right: Methane flux through different cross-sections.

3.2.2 Emission Uncertainty

The uncertainty of the emission rate estimated with the CSF method is considered to consist of three components, which are combined by adding their variances, assuming they are uncorrelated. These components include:

- **Wind Uncertainty:** Temporal variability in wind speed is accounted for by using the standard deviation of timesteps before and after the observation (-3h to +1h). Additionally, a constant uncertainty value of 0.5 m/s is added to represent overall wind uncertainty.
- **Dispersion:** This component accounts for turbulence and other effects leading to variability in the fluxes, as observed across the individual CSF cross sections (Fuentes Andrade, et al., 2024).
- **Other Error Terms, Including Algorithm Sensitivity:** A relative uncertainty of 20% is applied, based on numerical experiments where parameters or algorithm controls were varied. This represents the minimum achievable relative error for emissions derived from a single satellite overpass and includes the sensitivity of the algorithm.

3.3 Used Datasets

We use measurements from the hyperspectral imagers EnMAP (Guanter, et al., 2015), EMIT (Green, et al., 2020) and PRISMA (Loizzo, et al., 2018). All three instruments use push broom method to cover a scene with a grid of ground pixels. For each ground pixel a spectrum is measured that covers parts of the visual and near infrared (VNIR) and short-wave infrared spectral range. More details are given in Table 1.

	EnMAP	EMIT	PRISMA
Spectral range	420-1000 nm (VNIR) and 900-2450 nm (SWIR)	380 – 2500 nm	405-980 nm (VNIR) and 940-2500 nm (SWIR)
Spectral sampling (@2200nm)	~10 nm	~7.5 nm	~8nm
FWHM (@ 2200nm)	~8nm	~8.5nm	~10nm
Spatial sampling	30m, swath 30km	60m, swath ~75km	30m, swath 30km
Orbit	sun sync at ~11:00 local time	ISS	sun sync. at ~10:30 local time
Launch date	1. April 2022	14. July 2022	22. March 2019

Table 1: Overview over the satellite missions used in this TN.

3.4 Target Selection

Searching the full archive of all available scenes measured by EMIT, EnMAP, and PRISMA for emission sources is currently infeasible due to limited data access and the challenge of identifying small, unknown point-source plumes within the data. Therefore, we have used prior knowledge of potential target locations to guide our search for emission plumes.

A main source of targets is given by the Carbon Mapper data portal (<https://data.carbonmapper.org>), which provides information on detected emission plumes and their emissions from a variety of instruments, including EMIT. For this study, we utilize all detected methane emission plume locations from EMIT measurements available on the portal, up until January 14, 2025 (Figure 2). It should be pointed out that EMIT observations are limited to $\sim\pm 52^\circ$ latitude due to the ISS orbit. Note that the portal has recently been extended to also include data from the Tanager satellite mission. Additional locations found with Tanager have not been included here.

Additionally, we incorporate a list of coal mine ventilation shafts in the Upper Silesian Coal Basin, provided by (Gałkowski, et al., 2021). We use 53 locations categorized as “Active Coal Mines Reporting Emissions” or “Inactive/Closing Coal Mines Reporting Emissions”.

For each target location, we have searched the data portals of EMIT, EnMAP and PRISMA for measurements. In case of PRISMA and EnMAP, it is also possible to make observation requests for specific locations. For EnMAP, we have submitted observations request for the identified locations (but so far only one request has been carried out). A list of target locations and the number of available satellite observations is given in Table 2.



3.5 Data Processing

We identified all EMIT, EnMAP, and PRISMA measurements that include at least one of the known target locations. These measurements were then downloaded, provided they had less than 20% cloud cover. For EMIT, we also obtained measurements with plumes detected by Carbon Mapper, regardless of cloud cover.

We have obtained all images listed in Table 2. However, unlimited and easy data access is only available for EMIT. For PRISMA and EnMAP, data access via their web portal is more restricted. Furthermore, in case of PRISMA, data download is limited to 5 scenes/day, while for EnMAP there can be several days delay between order and possible download for measurements from their catalogue. Another problem is that the cloud mask provided in the L1 data is not reliable for PRISMA so that clouds are often not marked correctly.

For each scene, methane enhancement maps are generated using the three HiFi retrieval methods described above. The resulting maps are analysed, and the likelihood of a valid plume is assessed based on the following criteria.

- Enhancement: Is a similar enhancement visible with all three retrieval methods?
- Plumelike: Does the enhancement have a plume-like shape?
- Wind direction: Does the apparent plume direction match the ERA5 10m wind direction?
- Surface: Is the plume similar to surface features in the scene?
- Plausible source: Is there a plausible emission source (according to E-PRTR, (Gałkowski, et al., 2021), google maps)
- Cloudy: Is the apparent plume affected by the presence of clouds?

We assign each criteria a score and if the total score is equal or above a threshold (here chosen as 2), then we assume that we most likely observed a plume. The full list of scores for each evaluated scene is given in Table 6.

For all locations where a likely plume is detected, we then determine whether emission estimation using the CSF method is feasible or not based on the following criteria (if a criterion is not fulfilled then we do not carry out an emission estimation):

- Too many missing ground pixel
- Local methane accumulation due to low wind speed and/or terrain features.
- Large change in wind direction across a plume



4. Results & Discussion

4.1 Comparison of three Retrieval Methods

Since the HiFi retrieval software includes three different retrieval methods for CH₄ enhancements, we can assess results obtained from all three methods against each other.

One example for Bari, Italy from EMIT is shown in Figure 3. We can see all three methods produce a clear plume feature. However, the methods lead to different levels of background noise with the lowest noise being found for the matched filter method and the highest noise for the albedo (PhysicsF) method. The albedo method also shows a higher plume enhancement compared to the other two methods. The lower panel of Figure 3 shows a RGB image and the surface brightness derived from EMIT itself. Also shown is a google satellite image (not from same day). These images show that in this example the plume does not correlate with surface features.

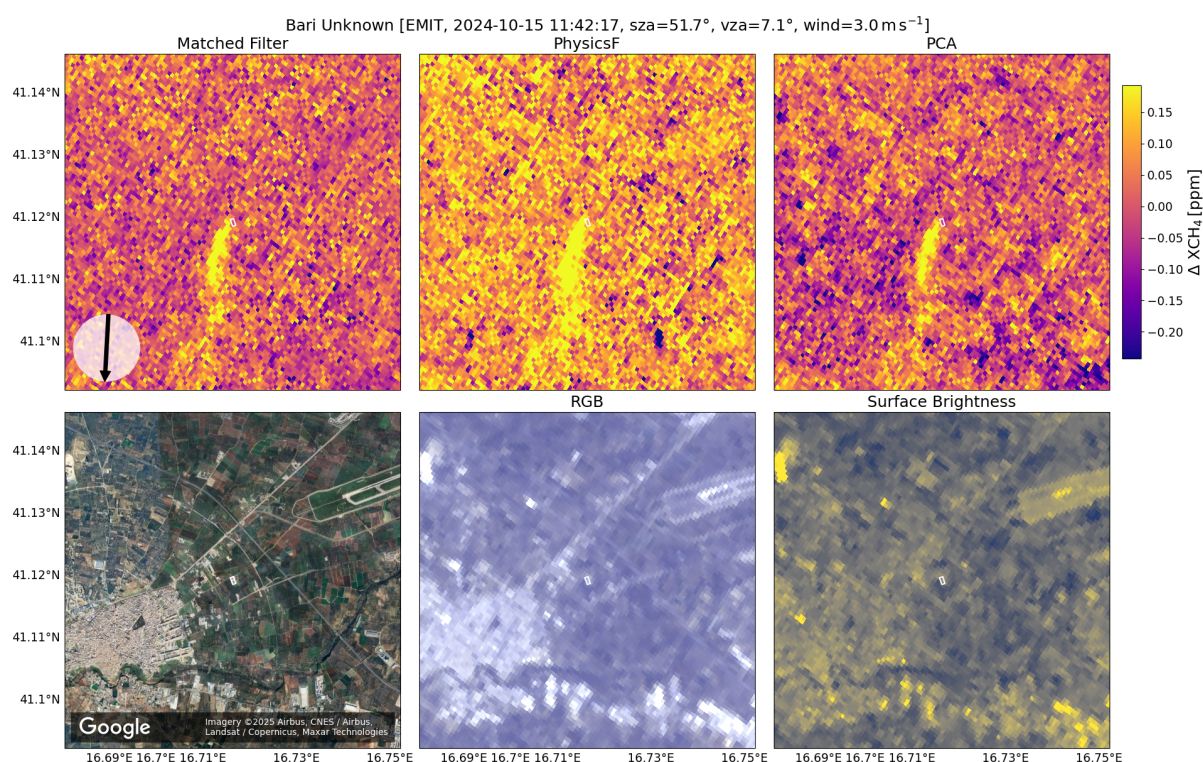


Figure 3: Top row: ΔXCH_4 map for the three retrieval methods, with the black arrow indicating the ERA5 10m wind direction. Bottom left: Satellite image. Bottom centre: RGB image derived from the measured spectrum. Bottom right: Surface reflectance estimated from the spectrum.

A second example over Lisbon, Portugal is given in Figure 4. This example illustrates that the three methods have different sensitivities to surface interference with the matched filter method showing fewest features. We can see that at the northern edge of the landfill (indicated by the white polygon) the apparent CH₄ enhancement feature coincides with a bright roof that is visible in the satellite, RGB and surface brightness image. Also, the large rectangular feature south east of the landfill coincides with a solar power plant. A small enhancement is visible on southern edge of the landfill which could be an emission from the landfill that is too small to be analysed using the CSF method.

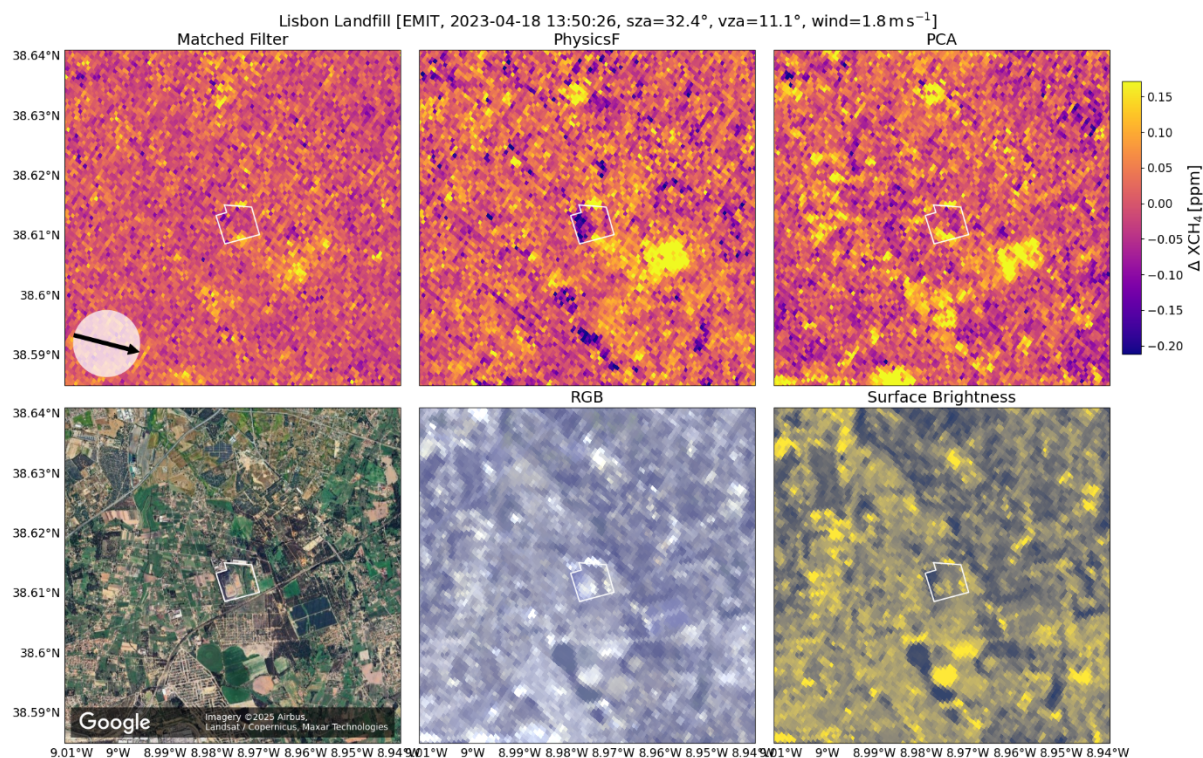


Figure 4: As Figure 3 but over Lisbon, Portugal

From our comparisons, we conclude that the matched filter method most often gives the most reliable result among the three methods. Thus, we have used the results of the matched filter retrieval for the estimation of emission values. However, the comparison between the three methods is used as a criterion of the plume identification procedure described above.

4.2 Comparison of CH₄ enhancement retrievals from the three satellite missions

A comparison of measurements by the three different instruments for a small section of an overlapping scene is shown in Figure 5. The measurements are for similar sun zenith angles and surface albedos but for different dates. The scenes have been retrieved with the matched filter method and are not over an emission location so that the scatter in the data can be estimated:

- EnMAP: $\sigma = 0.097$ ppm (SZA = 41°, albedo = 0.17, date: 2023-09-23 09:55)
- EMIT: $\sigma = 0.051$ ppm (SZA = 38°, albedo = 0.14, date: 2024-07-26 13:02)
- PRISMA: $\sigma = 0.321$ ppm (SZA = 36°, albedo = 0.14, date: 2020-04-09 09:25)

We find that EMIT has the best performance with a standard-deviation of the XCH₄ data of 51 ppb and a somewhat lower performance for EnMAP with a standard-deviation of 97 ppb. The lowest performance is found for PRISMA with a standard-deviation of 321 ppb. In addition, we find white stripes in the PRISMA measurement due to data being flagged as invalid in the L1 data. This feature is systematic in all PRISMA measurements.

Although we obtained a good number of PRISMA observations over the target locations, we did not positively identify plumes in PRISMA measurements due to its relatively high measurement noise and the systematic features in the L1B data. Thus, no results from PRISMA will be given in the following sections.

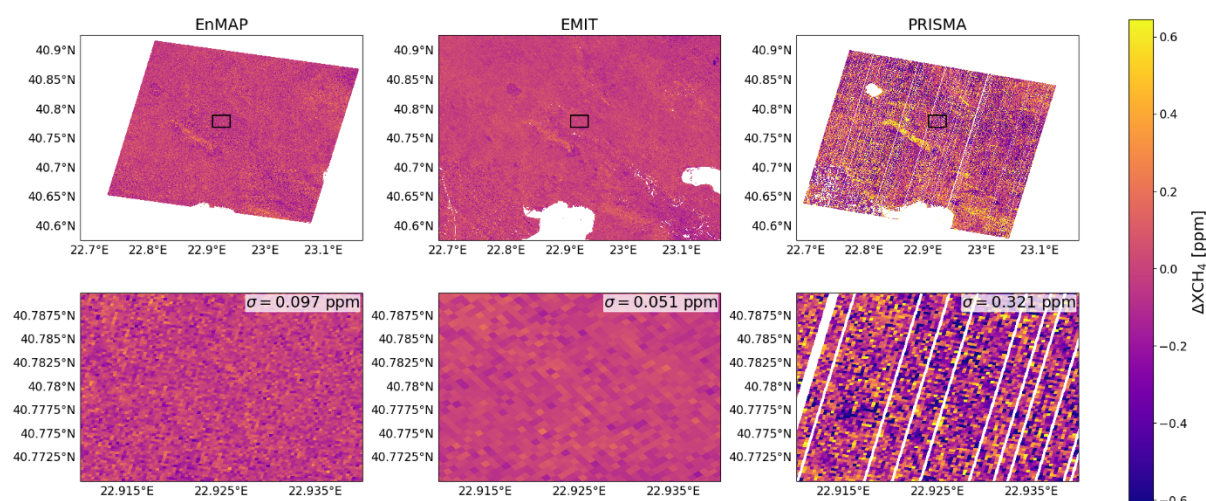


Figure 5: Comparison of XCH₄ enhancements with the different three imagers EnMAP, EMIT and PRISMA for a scene near Thessaloniki. The top row shows the retrieved XCH₄ for a large area. The black rectangle indicates the position of the analysed area shown enlarged in the bottom row.

4.3 Plume Scoring

We have classified all retrieved scenes according to the parameters described above. The full scoring of all retrievals is given in Table 6. Here, the retrieval of an EnMAP measurement over the Las Dehesas landfill site is used as an example to illustrate the plume scoring (Figure 6).

Explanation of plume score:

- Enhancement: all three methods show a similar, strong enhancement feature (result: +)
- Plumelike: feature does not show a clear plume-like shape along the wind direction (result: o)
- Wind direction: most likely plume direction is south to north (or north to south), more than 45° deviation from 10m wind direction (result: o)
- Surface: some parts of the feature correlate with bright areas on the landfill, but this cannot explain all of the enhancement (result: o)
- Plausible source: The emission likely originates within the landfill area. Other measurements of the landfill show a source at the centre of the eastern edge. (result: +)
- Cloudy: no clouds are visible in this small cut-out. However, other areas of the measurement contain clouds that could potentially affect the matched filter results. (result: o)

In total, we have assigned a score of 2, which is equal to our threshold for plume detection and thus we label this case as a ‘detected plume’.

As a second step, we carry out an assessment if an emission rate can be derived. In this case, we conclude that enhancement is probably a result of accumulation due to the low 10m wind speed of 0.3 m/s and the location of the landfill between hills. The CSF method depends on the flux through the cross sections perpendicular to the wind direction which is not fulfilled in case of local accumulation (result: -).

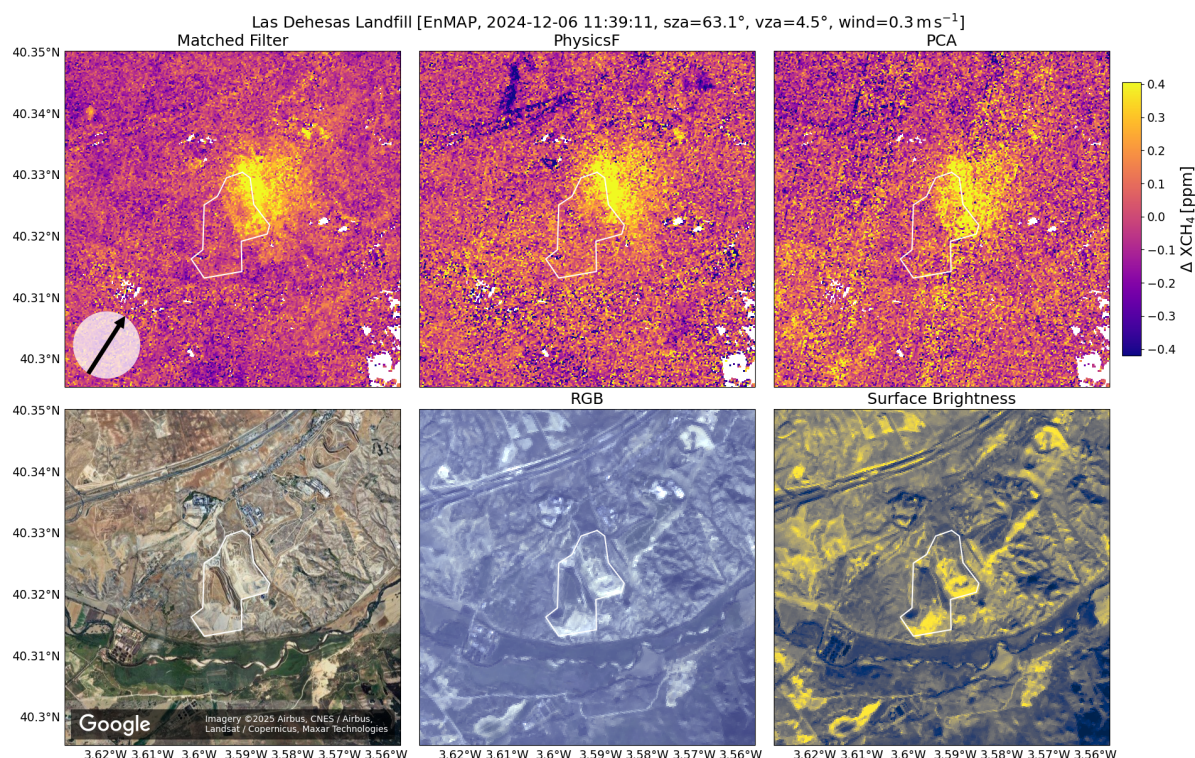


Figure 6. Top: XCH₄ enhancement retrieved over the Las Dehesas landfill site with the 3 retrieval methods of HiFi. Bottom: satellite image (google), RGB image and surface albedo.

4.4 Plume results

In total, using the criteria described above, we have detected 34 plumes in EnMAP and EMIT scenes (see also Table 6 in 8. Appendix). As already mentioned before, no plumes have been identified in PRISMA data. Also, for four locations, we did not detect a plume. A summary of the number of plumes detected for the different locations is given in Table 3 and Figure 7.

		EMIT	EnMAP		
Location	Type	No	No	Latitude [°]	Longitude [°]
Glina (Bucharest)	Landfill	0	0	44.3821	26.2201
Vidra (Bucharest)	Landfill	1	1	44.3171	26.1265
Lisbon	Landfill	1	1	38.6131	-8.9756
Pinto (Madrid)	Landfill	2	2	40.2636	-3.6341
Las Dehesas (Madrid)	Landfill	0	5	40.3230	-3.5929
Murcia	Landfill	0	0	37.9861	-1.2912
Granada	Landfill	0	0	37.0537	-3.7110
Hellín	Unknown	1	0	38.4981	-1.6788
Thessaloniki	Landfill	2	2	40.8478	23.0803

Athens	Landfill	1	0	38.0731	23.6550
Larissa	Landfill	0	0	39.7985	22.4241
Istanbul	Landfill	1	0	41.2156	28.1503
Vinča (Belgrade)	Landfill	1	0	44.7852	20.5969
Padua	Unknown	0	0	45.2436	12.0316
Bari	Unknown	1	0	41.1193	16.7164
Upper Silesian Coal Basin	Coal Mine	10	2	-	-

Table 3: List of plumes detected for the selected target locations.

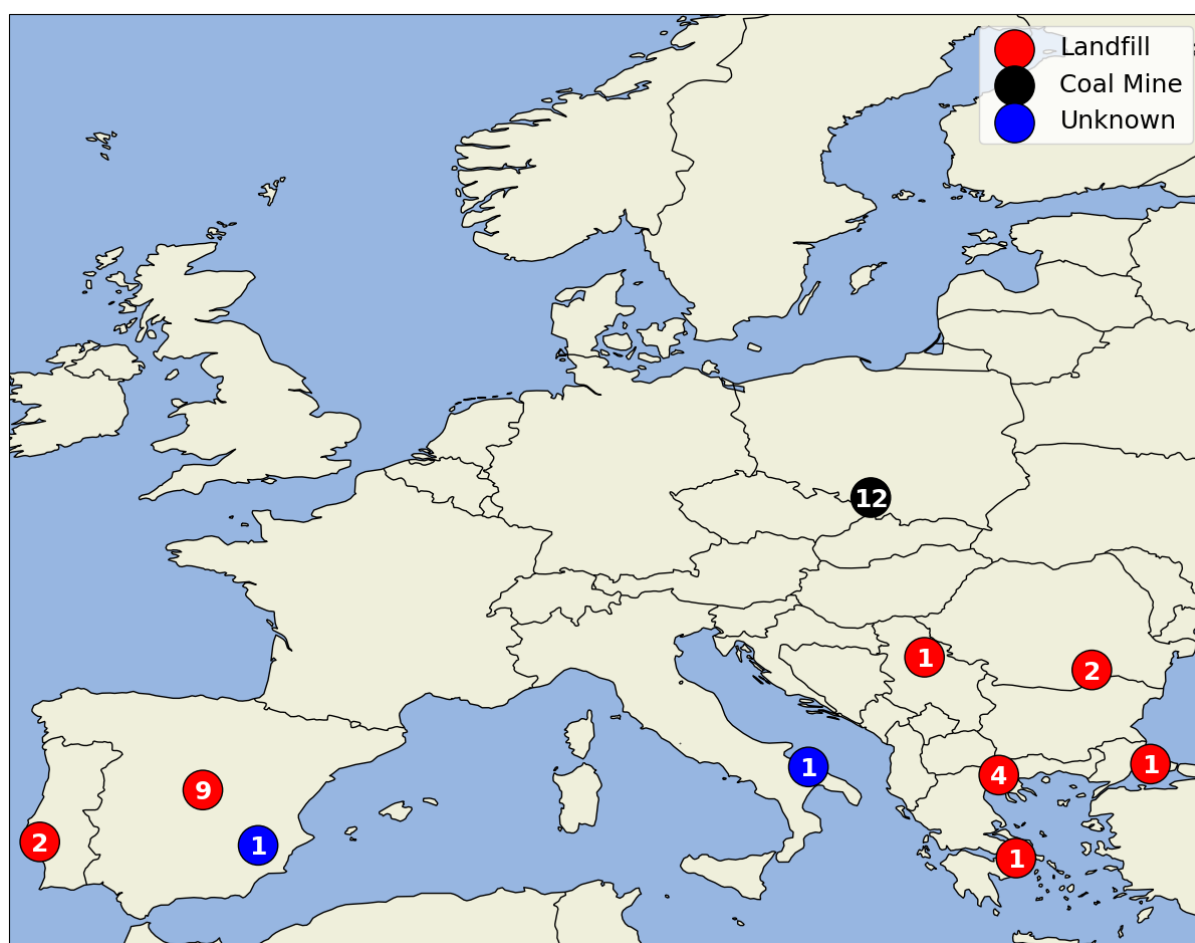


Figure 7: Location and number of methane plumes identified in EMIT and EnMAP measurements.

The retrieved CH₄ enhancements for all detected plumes are shown in Figure 8 to Figure 10. All displayed results are for the matched filter method only. 20 images are for landfills and 12 images for coal mines. For the two locations Bari and Hellin, no known source could be identified. The shape of the landfills is indicated by a white polygon while coal mine ventilation shafts are shown as black dots. In all shown cases, we have identified a plume signal but the spatial extend and the observed magnitude of the enhancement varies greatly. Some features will be discussed in the following.

In some cases, we observe a very large accumulation of CH₄ that is due to very low 10m wind speed (Figure 8 D and I and Figure 9 C). In such cases, it will not be possible to determine a reliable emission

value. For some landfill sites we have multiple plume measurements and we find that the plume origin is located in a similar part of the landfill, for example for the Las Dehesas landfill in Figure 8 E to H we observe the origin in the middle of the eastern border. Coal mining ventilation shafts can be spatially close, e.g. Zofiowka_shaft_IV and Zofiowka_shaft_V are located close together (~350m) so that we don't distinguish between them (here only Zofiowka_shaft_V is used). As shown in Figure 10 E, the emission plumes from both shafts are well aligned in wind direction. For some of the measurements, a large fraction of data is missing due to low sun zenith angle and/or dark surface (Figure 10 B and Figure 10 F). For example, the white band in Figure 9 I is the Danube river. In some cases, clear surface interference is visible, e.g. in Figure 10 H to Figure 10 L streets can be seen as bright lines. These surface features are difficult to separate from the observed plumes which prevents an emission estimate for these cases.

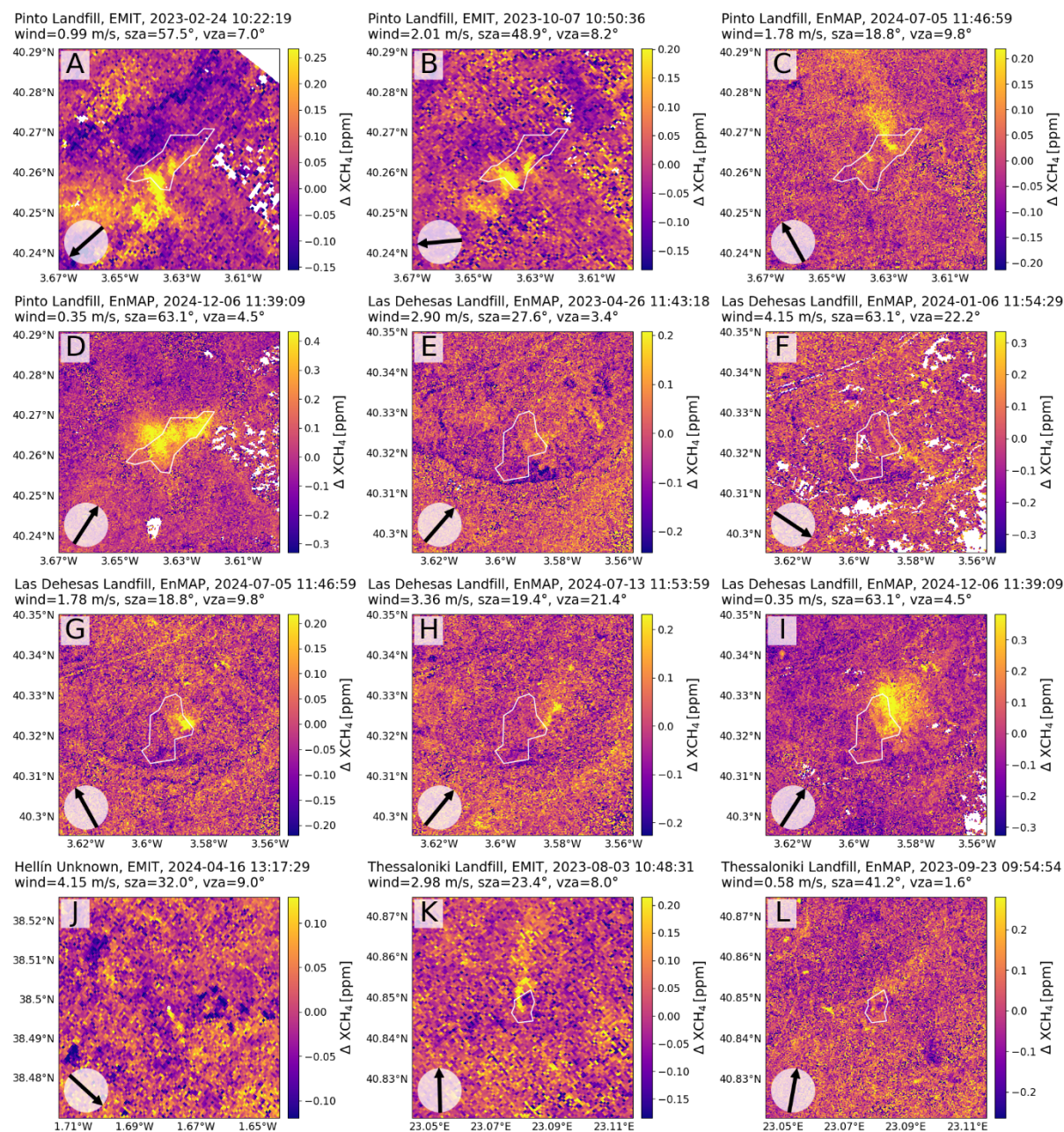


Figure 8: ΔXCH_4 retrieved with our Matched Filter method for different targets. The black arrow indicates the ERA5 10m wind direction. White lines show an approximate border of the landfill.

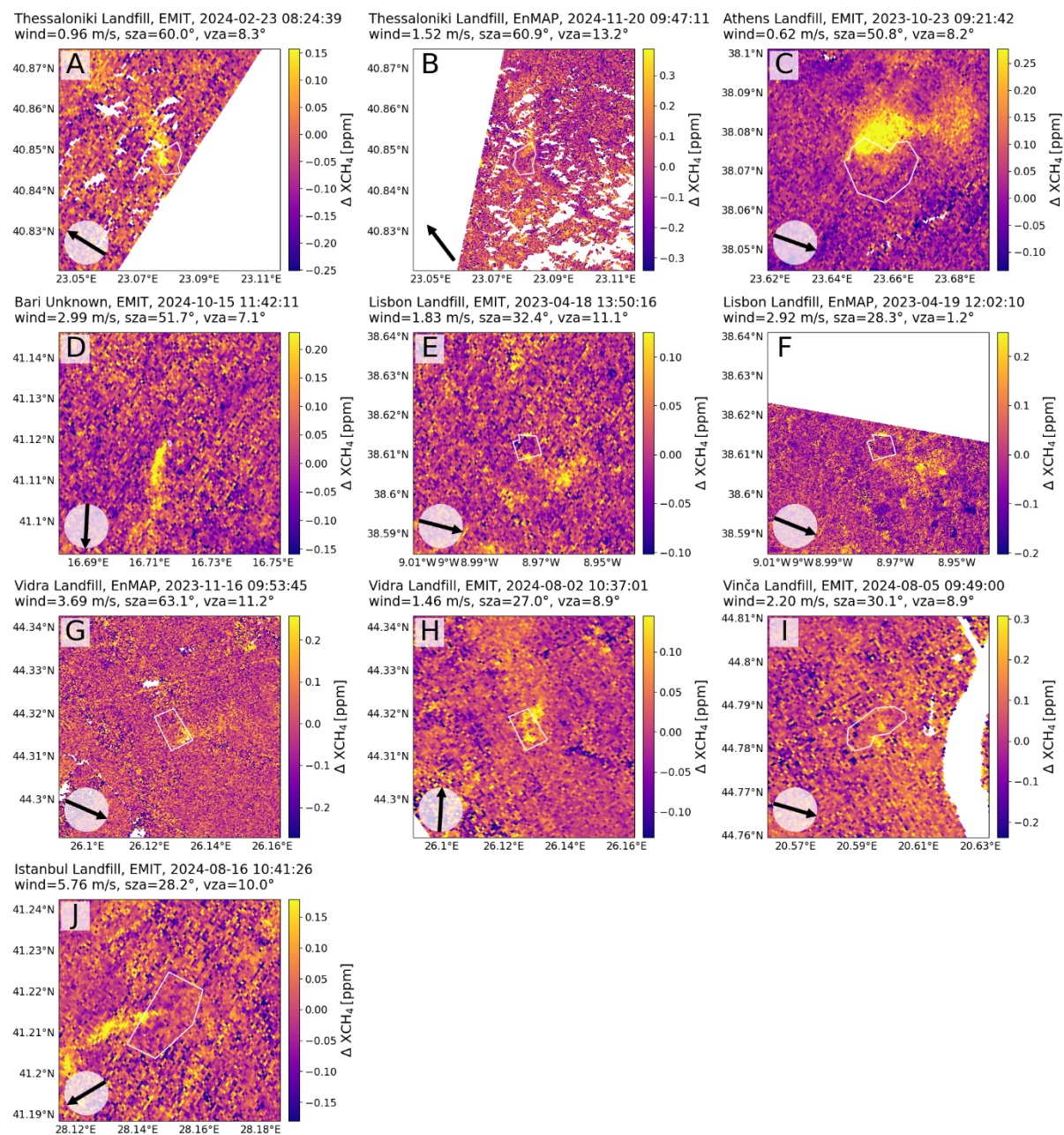


Figure 9: As Figure 8 for more targets.

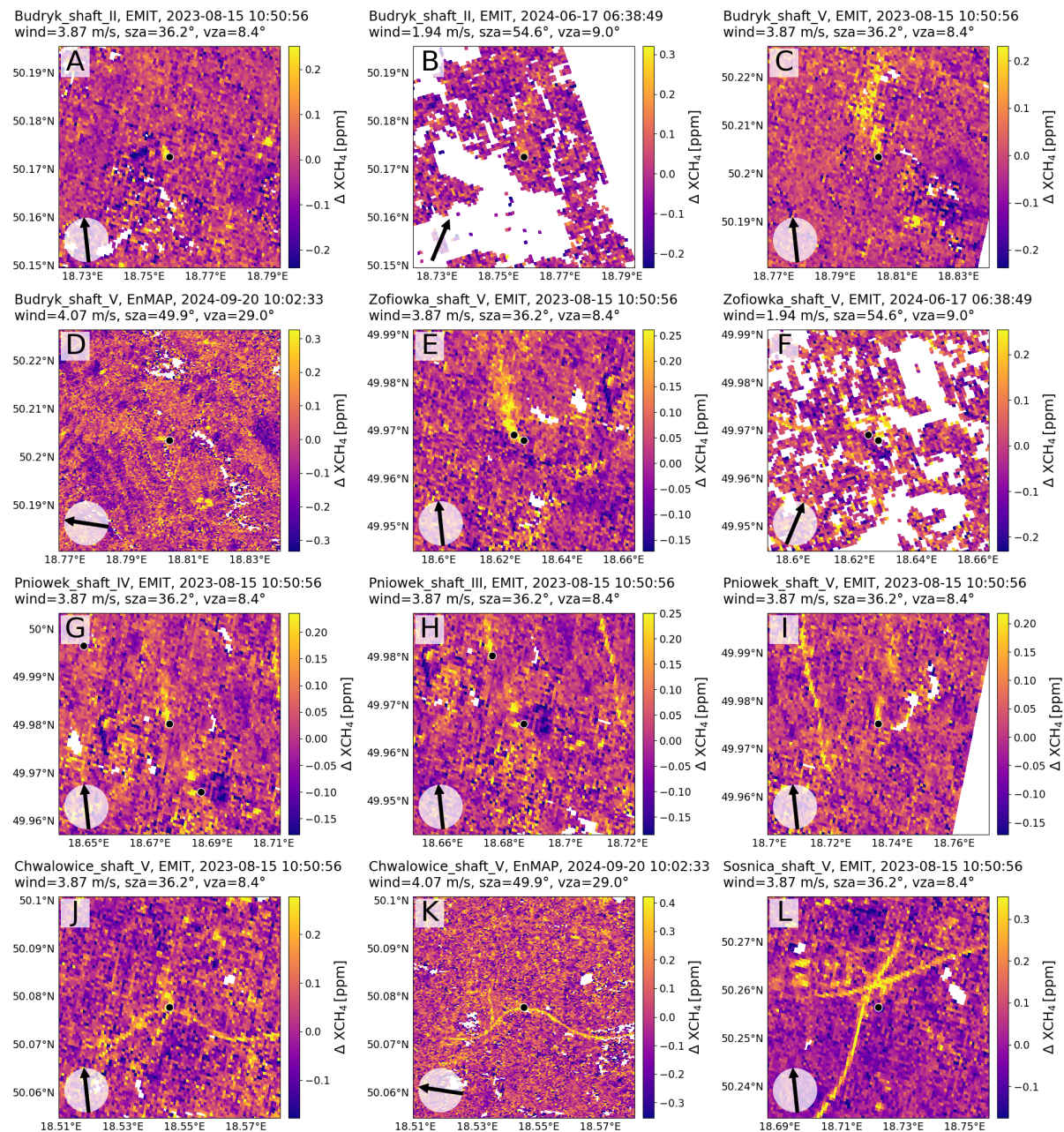


Figure 10: As *Figure 8* for more targets. Black dots show approximate position of ventilation shaft.

4.5 Comparisons of HiFi (EMIT) with Carbon Mapper (EMIT)

The availability of CH₄ retrievals from EMIT on the Carbon Mapper portal allows a direct comparison with the HiFi retrieval presented in this deliverable. In the following four different examples will be discussed.

4.5.1 Example Unknown target near Bari (Italy)

The comparison between the XCH₄ enhancement retrieval with HiFi and from the Carbon Mapper team is shown in *Figure 11*. We find in both cases a similar plume and the derived emission values are 5.19 ± 1.90 t/h and 4.93 ± 0.42 t/h from HiFi and Carbon Mapper, respectively. Both estimates have used different windspeeds (HiFi: 3.24 m/s from ECMWF ERA5; Carbon Mapper: 3.06 m/s from ECMWF

forecast). If we use the same windspeed then the HiFi estimate changes to 4.90 t/h which is almost identical to the Carbon Mapper value.

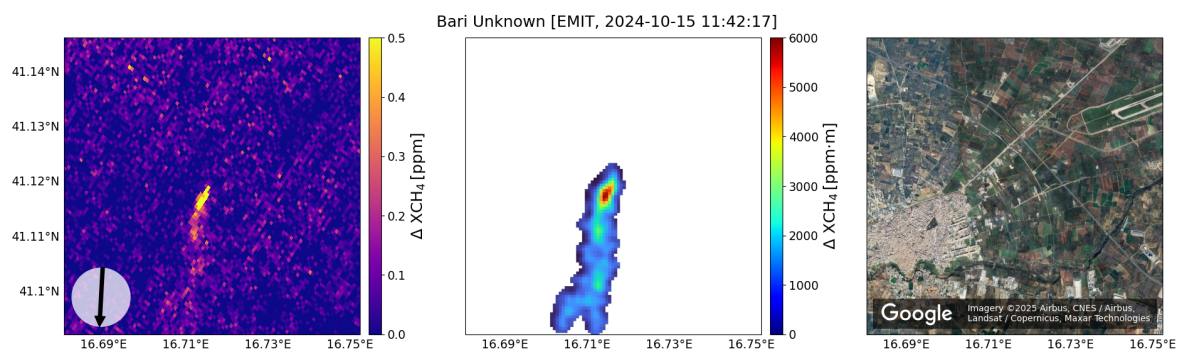


Figure 11: Left: HiFi result; Centre: Carbon Mapper (plume images are provided on the Carbon Mapper data portal smoothed, sampled, with plume mask already applied and with different units); Right: satellite image

4.5.2 Example Istanbul landfill

For the Istanbul landfill, again a similar plume is observed with HiFi and by Carbon Mapper (Figure 12). We have found the highest emission values of 6.82 t/h for the Istanbul landfill. It is also the scenario with the highest windspeeds (6.47m/s according to ECMWF ERA5). The Carbon Mapper emission value of 3.57 t/h is substantially lower. The wind speed used by the Carbon Mapper team (5.15 m/s) is also lower than assumed in HiFi. Using the Carbon Mapper windspeed lowers the emission value to 5.42 t/h, but this is still much higher than found by Carbon Mapper so that we are left with a discrepancy between both estimates that cannot be easily resolved.

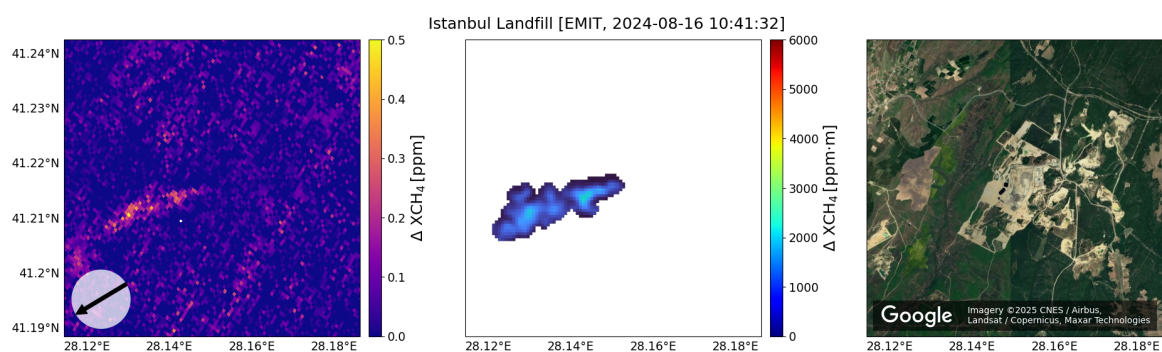


Figure 12: As Figure 11 but for a landfill near Istanbul

4.5.3 Example Athens landfill

For the Athens landfill, both HiFi and Carbon Mapper show a strong CH₄ enhancement feature with a large spatial extent (Figure 13). This plume shows characteristics of a local accumulation due to low windspeed (here: 0.62 m/s) and hilly terrain. Similar to other plumes under comparable conditions in Figure 8 Panels D and I (Figure 9 Panel C is the Athens landfill). Due to this accumulation of CH₄, the assumption of the applied flux method, that transport is dominated by advection, is no longer valid and we have flagged this scene as unsuitable for emission estimation. The Carbon Mapper team has decided to give an estimate of the emission for this scene (2.49 ± 0.52 t/h).

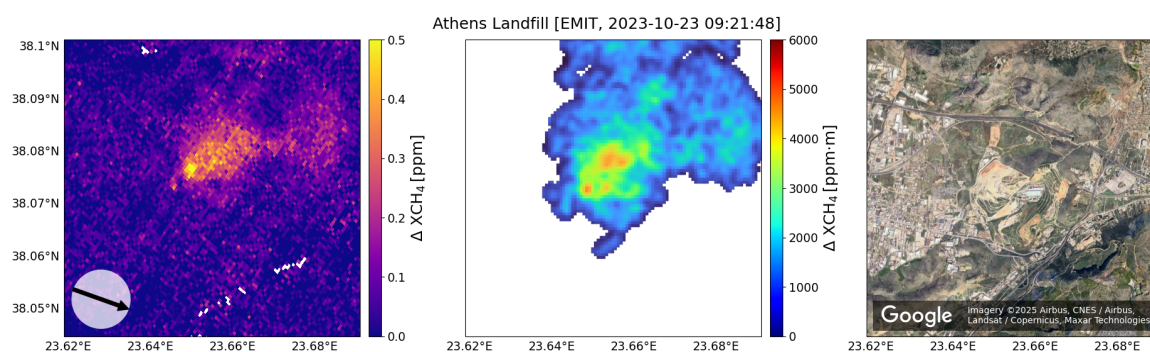


Figure 13: As Figure 11 but for a landfill near Athens

4.5.4 Example Murcia landfill

The Carbon Mapper portal reports a plume for a landfill near Murcia. The scene given in the portal has also been analysed with HiFi and the resulting CH₄ enhancement is shown in Figure 14. Several very localised spots of enhanced CH₄ can be seen in the HiFi result but they tend to correlate with Buildings or other surface structures at the edge of landfill and with the height profile in the landfill. Thus, we have not classified this scenario as a robust plume signal.

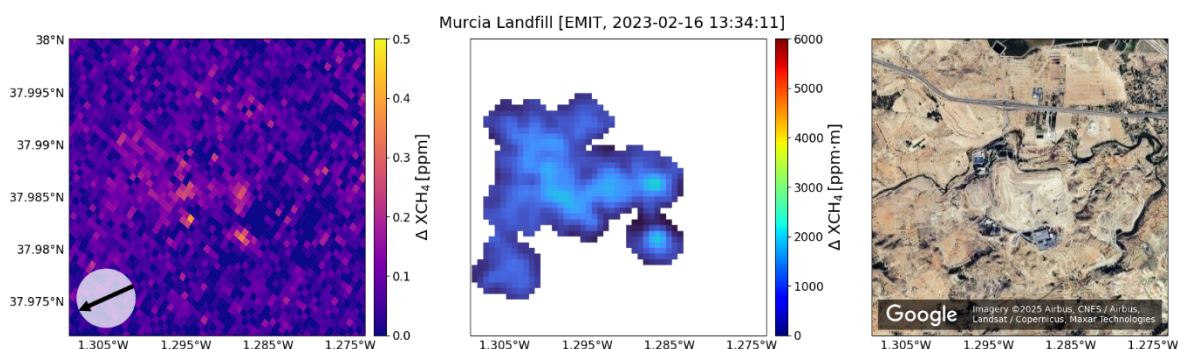


Figure 14: As Figure 11 but for a landfill near Murcia.

4.6 Estimation of Emissions

From the 34 detected plumes, we have estimated emissions for 12 landfill plumes (including Bari and Hellín) and 6 plumes related to ventilation shafts. This selection is based on the criteria given in section 3.5 (see also Table 6 in 8. Appendix). The rotated and resampled plumes together with the fluxes through the individual cross-sections and the resulting emission estimates are given in Figure 15 and Figure 16. From the different fluxes through the cross-sections through a plume, the mean flux is calculated. Variations of the derived fluxes for different cross-sections of a plume reflect the effects of turbulence, statistical retrieval errors and of surface interference patterns. From the variation of the flux through the cross section a statistical error is derived which forms one component of the total error assigned to the final flux estimate.

Although, as one of the selection criteria, we screen out plumes that are significantly bent, we still find cases that show a distinct change in direction across the plume. One example is shown in Figure 15 I.

Here the plume bends after ~600m and the new direction deviates by ~25° from the original direction. This results in a worst-case error of about 10% (this error is not included in the error budget).

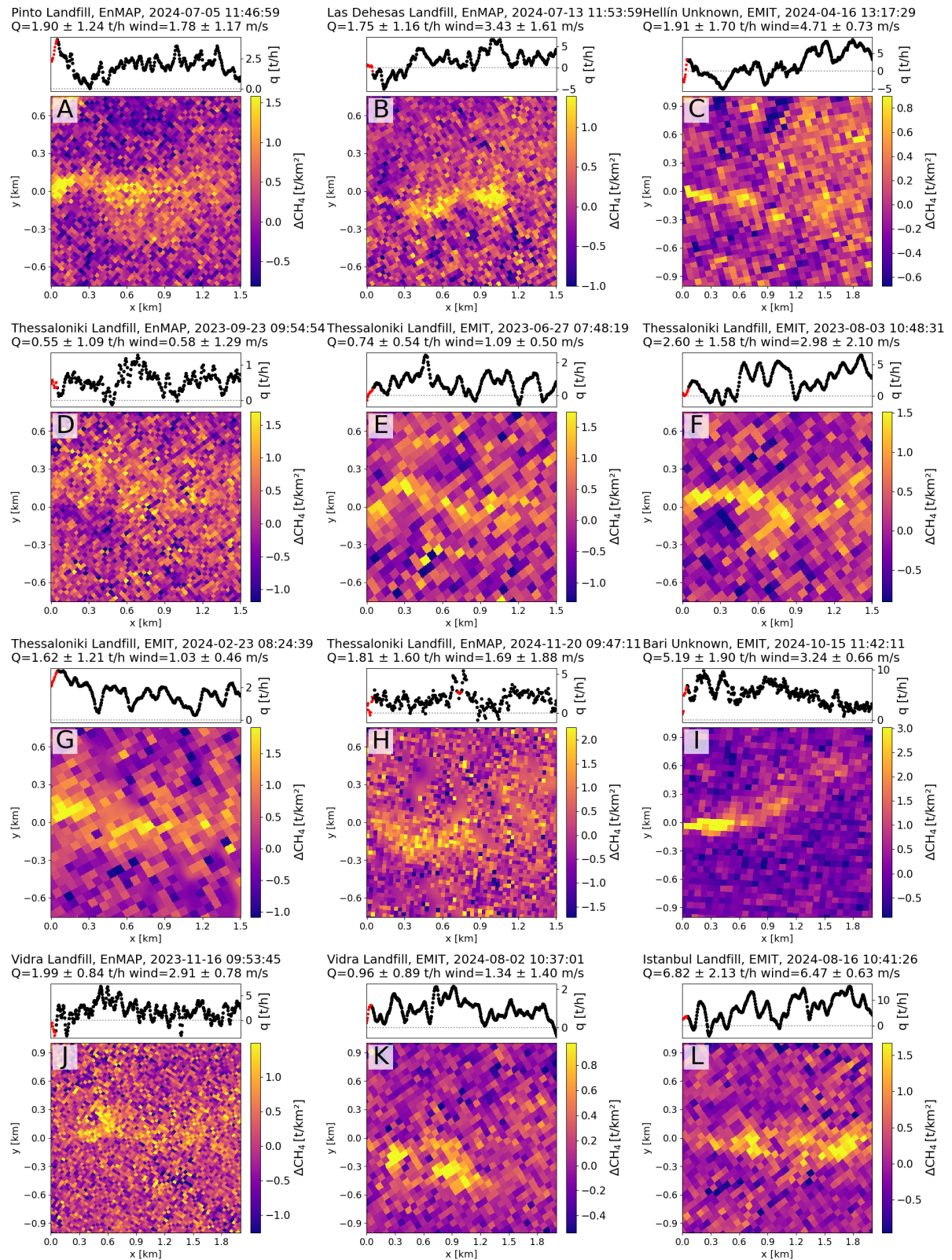


Figure 15: ΔXCH_4 enhancement and flux through cross-sections.



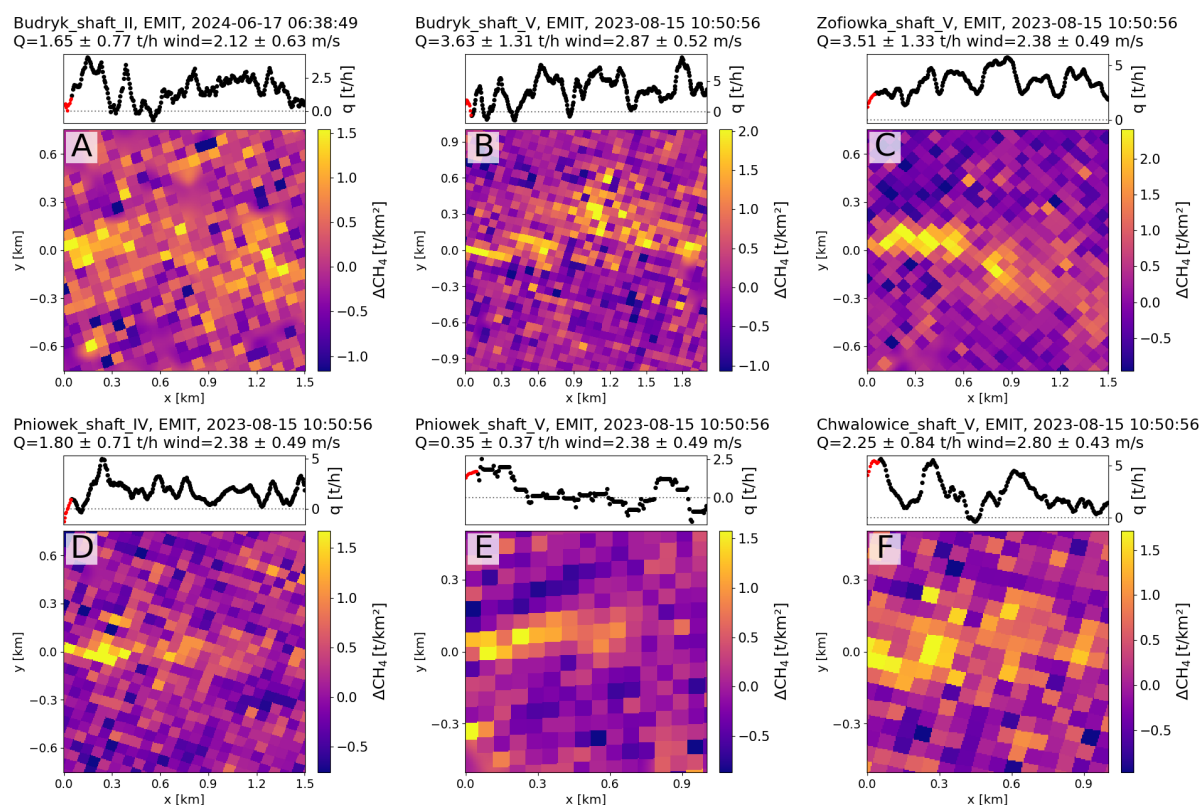


Figure 16: As Figure 15

The derived emission estimates for the different landfill locations are summarised in Table 4. The table includes

- HiFi: our emission rates result and the associated uncertainty. Value in () is the statistical uncertainty due to variability in cross-sections only.
- Carbon Mapper (EMIT): emission rates and uncertainty for the same EMIT data as used by HiFi (data download: January 14, 2025)
- Carbon Mapper (Tanager): emission rates and uncertainties from Tanager measurements (based on uncalibrated first light measurements; data download: February 25, 2025). Tanager data is only available since mid/end of 2024. Carbon Mapper only specifies coordinates as source location. We have identified the most likely targets by finding the nearest entry in our target list (Table 2).
- GHGSat: data taken from (Dogniaux & Crevoisier, 2024), based on GHGSat measurements between 2021 and 2022.
- E-PRTR: reported emission for 2022 (<https://doi.org/10.2909/ff47e25d-5d4c-491d-b9ce-de17ca61fe6d>)

Location	Scene	Emission rate [t/h]				
		HiFi (Our study)	Carbon Mapper (EMIT)	Carbon Mapper (Tanager)	GHGSat (2021 - 2022)	E-PRTR 2022
Pinto Landfill	EnMAP_20240705T114659	1.90±1.24 (0.44)	-	1.28±0.37	4.48±0.57	0.04
Las Dehesas Landfill	EnMAP_20240713T115359	1.75±1.16 (0.94)	-	1.77±0.74	2.98±0.42	0.17
Hellin Unknown	EMIT_20240416T131729	1.91±1.70 (1.66)	2.09±0.15	-	-	-
Thessaloniki Landfill	EnMAP_20230923T095454	0.55±1.09 (0.13)	-	1.83±0.56	2.91±0.99	0.68
	EMIT_20230627T074819	0.74±0.54 (0.20)	-			
	EMIT_20230803T104831	2.60±1.58 (0.82)	2.31±0.61			
	EMIT_20240223T082439	1.62±1.21 (0.38)	1.62±0.32			
	EnMAP_20241120T094711	1.81±1.60 (0.43)	-			
Bari Unknown	EMIT_20241015T114211	5.19±1.90 (1.35)	4.93±0.42	-	-	-
Vidra Landfill	EnMAP_20231116T095345	1.99±0.84 (0.58)	-	-	2.15±0.58	0.05
	EMIT_20240802T103701	0.96±0.89 (0.23)	0.62±0.06			
Istanbul Landfill	EMIT_20240816T104126	6.82±2.13 (1.94)	3.57±0.49	-	7.21±0.99	-

Table 4: Summary of flux estimates for the landfill locations. Included are also the two unknown targets at Bari and Hellin. The table gives results from our study using EnMAP and EMIT data (HiFi), from the Carbon Mapper portal for EMIT data, from the Carbon Mapper portal for recent Tanager data (2024 and 2025), from GHGSat (Dogniaux & Crevoisier, 2024), and from emissions reported for 2022 in the E-PRTR inventory.

The HiFi emission estimates for the different landfills show a large range of values from 0.55 t/h to 6.28 t/h. The emission estimates have large uncertainties that can exceed 100%, but under favourable conditions can be as low as 31%. Note that the statistical uncertainty derived from the scatter of the fluxes through the different cross-sections is often much lower. With the exception of Thessaloniki and Vidra, we only have a single emission estimate for the different landfills. The two estimates for the Vidra site differ by about 100%, but they are observed 9 months apart and the uncertainties are large for both observations so that the two estimates agree within the assigned uncertainties. The emissions derived for the Thessaloniki landfill show an even larger range of values between 0.55 t/h and 2.6 t/h, with the lowest and highest estimates being only a few weeks apart. These variations may reflect the potential impact of changing environmental conditions on landfill emissions. However, uncertainties of the estimates are large which reflects the inherent challenges involved in estimating emissions from hyperspectral sensors.

The Carbon Mapper portal provides emissions estimates from EMIT observations allowing direct comparisons for the same EMIT scenes. In general, we find that the estimates are in very good



agreement and differences are within assigned uncertainties. The exception is the Istanbul landfill, which will be discussed later on. It is also noteworthy that the uncertainties assigned to emissions by the Carbon Mapper team are significantly lower than by our HiFi method.

For some locations, emission estimates are also available from GHGSat for the time period 2021-2022 and from the recently launched Tanager mission (via the Carbon Mapper portal) for the time after mid 2024. For the two landfills near Madrid (Pinto and Las Dehesas), we find comparable emissions estimates from Tanager, while GHGSat reports substantially higher emission values. The Tanager measurements are for a similar time period as the EnMAP measurement we use, while the GHGSat observations have been taken much earlier so that this might indicate that emissions have dropped between 2021/2022 and 2024/2025. For the Thessaloniki Landfill, the emission value of 2.91 t/h from GHGSat is again higher than that derived from Tanager of 1.83 t/h, but both are roughly consistent with the range of values of 0.55 t/h and 2.6 t/h derived with HiFi. For the Vidra landfill, the GHGSat emission estimate of 2.15 t/h is similar but slightly higher than the higher of the two values derived with HiFi. Similarly for the Istanbul landfill, the GHGSat value is again slightly higher than the value derived with HiFi. In summary, we find that GHGSat values (for 2021-2022) tend to be higher than those derived with HiFi (for 2023-2024) while Tanager estimates (2024-2025) are roughly consistent with the HiFi values.

Landfill operators are required to report annual emission to the E-PRTR. The emissions values given in E-PRTR are in almost all cases much lower than observed by HiFi. Only for the Thessaloniki Landfill does the report value fall within the range of derived emissions with HiFi.

The emission estimates derived with HiFi for the coal mining ventilation shafts are given in *Table 5*. We find the emission values can vary between 0.35 t/h and 3.63 t/h. Emission estimates are available from Tanager for several of the shafts. The Tanager values vary over a similar range as observed with HiFi. In some cases, the Tanager estimates are similar to the HiFi estimates, but in other cases, the agreement is poor. This is not surprising as methane emissions from ventilation shafts can show large day-to-day variations (Swolkień, et al., 2022) and the Tanager data has not been acquired at the same time as the EMIT data.

Name	Scene	Emission rate [t/h]				
		HiFi	Carbon Mapper (Tanager)	E-PRTR 2018	WUG 2018	In situ 2018
Budryk_shaft_II	EMIT_20240617T063849	1.65±0.77 (0.43)	-	4.47	4.68	1.85
Budryk_shaft_V	EMIT_20230815T105056	3.63±1.31 (0.89)	2.93±0.77	4.47	4.68	2.01
Zofiowka_shaft_V	EMIT_20230815T105056	3.51±1.33 (0.75)	0.27±0.06 4.34±0.46	1.59	1.44	2.13
Pniówek_shaft_IV	EMIT_20230815T105056	1.80±0.71 (0.43)	0.36±0.15 2.03±0.45	2.08	2.28	0.91
Pniówek_shaft_V	EMIT_20230815T105056	0.35±0.37 (0.35)	1.32±0.35	2.08	2.28	1.40
Chwalowice_shaft_V	EMIT_20230815T105056	2.25±0.84 (0.61)	-	0.61	0.76	-

Table 5: Summary of flux estimates for the coal mining ventilation shaft. The table gives results from our study using EMIT (HiFi) and values for the year 2018 from (Gałkowski, et al., 2021) from E-PRTR and from the State Mining Authority (WUG). Also given are in-situ measurements by the State Mining Authority (WUG).



Emission rates for the observed coal mining shafts are also reported in (Gałkowski, et al., 2021). They provide values reported in E-PRTR for 2018 and values reported by the responsible State Mining Authority (WUG). Emissions reported on facility level are converted to emission rates for individual ventilation shafts. All shafts that belong to one facility have the same emission. (Gałkowski, et al., 2021) also report measured emission rates in-situ in some shafts. Values are from also from 2018. The annual emission values given by E-PRTR and WUG are similar but they can differ substantially from the in-situ observed emission values. The same is true when comparing the E-PRTR and WUG to our satellite measurement with HiFi. This is within our expectation as we are comparing an annual value with an observation on a single day.



5. Conclusion and outlook

We have evaluated methane point source emissions using hyperspectral satellite observations from PRISMA, EnMAP and EMIT. We have selected all cloud-free overpasses over 14 potential emission locations and retrieved CH₄ enhancements using the HiFi retrieval packages of IUP Bremen. We have defined a set of parameters to help us decide if a plume can be identified and if emission can be reliably estimated. Emissions have been estimated for 5 landfills, 2 unknown targets and 6 coal mining ventilation shafts. Assigned uncertainties of the emission estimates are high and range from 31% to over 100%. These uncertainties stem from statistical uncertainties of the retrieval, uncertainties of the wind data and systematic uncertainties of the applied method. A list of all detected plumes, and of all estimated fluxes has been generated with their associated uncertainties.

We have assessed the 3 different hyperspectral imagers and we find that PRISMA is not suitable for emission detection over European sources and we do not find positive detections with PRISMA. EMIT and EnMAP have a better performance than PRISMA and measurements from both sensors have allowed to detect emission plumes. Nevertheless, we have only managed to obtain a single emission value for most targets over a roughly two-year time period. This is due to the infrequent cloud-free observations provided by these sensors and the down-selection of data to allow robust estimation of fluxes.

For some instances, emission estimates exist from the Carbon Mapper portal for the same EMIT data as used by us. With the exception of an overpass over the Istanbul landfill, estimates from Carbon Mapper and us agree within their uncertainty ranges. Comparisons to recent Tanager measurements or to older GHGSat measurements is difficult as they are measured at different dates and we expect emissions to vary considerably. A similar problem arises when comparing our instantaneous estimate to annual emission values from inventories such as E-PRTP or WUG.

A major challenge is the sparseness of satellite data. The recently launched satellite missions Tanager and MethaneSAT together with the increasing fleet of GHGSat satellites will help to obtain more coverage. However, only Level 4 (flux estimates) data products from a single source will likely be available. Thus, there will be a continued need to derive emission estimates from publicly-available satellite data sources using transparent algorithms and methods.

In a future update of this report, we will extend the datasets of emission estimates from EMIT and EnMAP for European targets and synthesis our results with data from Tanager, MethaneSAT and GHGSat, depending on data availability. Furthermore, it is planned to expand beyond Europe and to include a case study with a focus on Russia. The two main target regions will be the North Caucasus (oil and gas) and the Kuznetsk Basin (coal). Details will be agreed with other WPs of the project.



6. Acknowledgement

This work has been supported by several IUP colleagues, especially Stefan Noel, Maximilian Reuter, Jonas Hachmeister and Michael Buchwitz. The method development also benefitted from co-funding from ESA (GHG-CCI+, MEDUSA, SMART-CH4) and nationally funded projects (ITMS).

In this deliverable data from the Carbon Mapper portal (<https://carbonmapper.org/>) is used in several instances. The data on the Carbon Mapper portal is provided by Carbon Mapper Inc. with funding from Bloomberg Philanthropies under a Modified Creative Commons Attribution ShareAlike 4.0 International Public License (<https://assets.carbonmapper.org/documents/Carbon-Mapper-Modified-Creative-Commons-License-21-11-09.pdf>).

We acknowledge the availability of satellite Level 1 data products from PRISMA (<https://www.asi.it/en/earth-science/prisma/>), EnMAP (<https://www.enmap.org>) and EMIT (<https://earth.jpl.nasa.gov/emit/data/data-portal/>).



7. References

- Dogniaux, M. & Crevoisier, C., 2024. Mapping the CO₂ total column retrieval performance from shortwave infrared measurements: synthetic impacts of the spectral resolution, signal-to-noise ratio, and spectral band selection. *Atmospheric Measurement Techniques*, September, Volume 17, p. 5373–5396.
- Fuentes Andrade, B. et al., 2024. A method for estimating localized CO₂ emissions from co-located satellite XCO₂ and NO₂ images. *Atmospheric Measurement Techniques*, February, Volume 17, p. 1145–1173.
- Gałkowski, M. et al., 2021. *Emissions of CH₄ and CO₂ over the Upper Silesian Coal Basin (Poland) and its vicinity*. s.l.:ICOS ERIC - Carbon Portal.
- Green, R. O. et al., 2020. *The Earth Surface Mineral Dust Source Investigation: An Earth Science Imaging Spectroscopy Mission*. s.l., IEEE.
- Guanter, L. et al., 2015. The EnMAP Spaceborne Imaging Spectroscopy Mission for Earth Observation. *Remote Sensing*, July, Volume 7, p. 8830–8857.
- Hersbach, H. et al., 2017. *Complete ERA5 from 1940: Fifth generation of ECMWF atmospheric reanalyses of the global climate*. s.l.:Copernicus Climate Change Service (C3S) Climate Data Store (CDS).
- Joyce, P. et al., 2023. Using a deep neural network to detect methane point sources and quantify emissions from PRISMA hyperspectral satellite images. *Atmospheric Measurement Techniques*, May, Volume 16, p. 2627–2640.
- Krautwurst, S. et al., 2024. Identification and Quantification of CH₄ Emissions from Madrid Landfills using Airborne Imaging Spectrometry and Greenhouse Gas Lidar. October.
- Krautwurst, S. et al., 2021. Quantification of CH₄ coal mining emissions in Upper Silesia by passive airborne remote sensing observations with the Methane Airborne MAPper (MAMAP) instrument during the CO₂ and Methane (CoMet) campaign. *Atmospheric Chemistry and Physics*, December, Volume 21, p. 17345–17371.
- Loizzo, R. et al., 2018. *Prisma: The Italian Hyperspectral Mission*. s.l., IEEE.
- Schneising, O. et al., 2020. Remote sensing of methane leakage from natural gas and petroleum systems revisited. *Atmospheric Chemistry and Physics*, August, Volume 20, p. 9169–9182.
- Schneising, O. et al., 2024. Towards a sector-specific CO/CO₂ emission ratio: satellite-based observations of CO release from steel production in Germany. *Atmospheric Chemistry and Physics*, July, Volume 24, p. 7609–7621.
- Swolkień, J., Fix, A. & Gałkowski, M., 2022. Factors influencing the temporal variability of atmospheric methane emissions from Upper Silesia coal mines: a case study from the CoMet mission. *Atmospheric Chemistry and Physics*, December, Volume 22, p. 16031–16052.
- Thompson, D. R. et al., 2015. Real-time remote detection and measurement for airborne imaging spectroscopy: a case study with methane. *Atmospheric Measurement Techniques*, October, Volume 8, p. 4383–4397.



Vanselow, S. et al., 2024. Automated detection of regions with persistently enhanced methane concentrations using Sentinel-5 Precursor satellite data. *Atmospheric Chemistry and Physics*, September, Volume 24, p. 10441–10473.



8. Appendix

Location	Scene	Enhancement	Plumelike	Wind direction	Surface	Plausible source	Cloudy	Plume Score	Emission Estimate
Pinto Landfill	EMIT_20230224T102219	+	0	0	0	+	0	2	-
Pinto Landfill	EMIT_20231007T105036	+	0	0	0	+	0	2	-
Pinto Landfill	EnMAP_20240705T114659	+	+	+	0	+	0	4	+
Pinto Landfill	EnMAP_20240713T115359	0	0	+	0	+	-	1	-
Pinto Landfill	EnMAP_20240927T112447	0	0	+	0	+	-	1	-
Pinto Landfill	EnMAP_20241206T113909	+	0	0	0	+	0	2	-
Las Dehesas Landfill	EnMAP_20230426T114318	0	0	+	0	+	0	2	-
Las Dehesas Landfill	EMIT_20231007T105036	0	0	0	0	+	0	1	-
Las Dehesas Landfill	EnMAP_20240106T115429	0	+	+	0	+	0	3	-
Las Dehesas Landfill	EnMAP_20240705T114659	+	+	-	0	+	0	2	-
Las Dehesas Landfill	EnMAP_20240713T115359	+	+	+	-	+	0	3	+
Las Dehesas Landfill	EnMAP_20240927T112447	+	0	0	0	+	-	1	-
Las Dehesas Landfill	EnMAP_20241206T113909	+	0	0	0	+	0	2	-
Murcia Landfill	EMIT_20230216T133401	0	0	0	-	0	0	-1	-
Murcia Landfill	EMIT_20230423T112619	+	0	0	-	0	0	0	-
Murcia Landfill	EMIT_20230604T115318	0	0	0	-	0	0	-1	-
Murcia Landfill	EMIT_20231008T100218	0	0	0	-	0	0	-1	-
Granada Landfill	EMIT_20230408T103156	0	0	0	-	0	0	-1	-
Hellín Unknown	EMIT_20240416T131729	+	+	+	0	-	0	2	+
Thessaloniki Landfill	EMIT_20230627T074819	+	+	-	-	+	0	1	-
Thessaloniki Landfill	EMIT_20230730T122521	0	0	0	-	+	0	0	-
Thessaloniki Landfill	EMIT_20230803T104831	+	+	+	0	+	0	4	+
Thessaloniki Landfill	EnMAP_20230923T095454	+	+	+	0	+	0	4	+
Thessaloniki Landfill	EMIT_20240223T082439	+	+	0	0	+	0	3	+
Thessaloniki Landfill	EMIT_20240726T130211	0	0	-	0	+	0	0	-
Thessaloniki Landfill	EnMAP_20241120T094711	+	+	0	0	+	0	3	+
Athens Landfill	EMIT_20231023T092142	+	0	0	0	+	0	2	-
Athens Landfill	EMIT_20240622T090851	+	0	0	-	+	0	1	-
Larissa Landfill	EMIT_20240803T094747	0	+	0	-	+	0	1	-
Padua Unknown	EMIT_20230823T091747	0	0	0	0	0	0	0	-
Bari Unknown	EMIT_20241015T114211	+	+	+	0	-	0	2	+



Lisbon Landfill	EMIT_20230418T135016	+	o	+	-	+	o	2	-
Lisbon Landfill	EnMAP_20230419T120210	+	+	+	-	+	o	3	-
Vidra Landfill	EnMAP_20231116T095345	+	+	o	o	+	o	3	+
Vidra Landfill	EMIT_20240802T103701	+	+	+	-	+	o	3	+
Vinča Landfill	EMIT_20240805T094900	+	+	o	-	+	o	2	-
Vinča Landfill	EMIT_20240809T081308	o	o	o	-	+	o	0	-
Istanbul Landfill	EMIT_20240611T064013	+	+	o	-	+	-	1	-
Istanbul Landfill	EMIT_20240816T104126	+	+	+	o	+	o	4	+
Budryk_shaft_II	EMIT_20230815T105056	+	+	+	o	+	o	4	-
Budryk_shaft_II	EMIT_20240617T063849	o	+	+	o	+	o	3	+
Budryk_shaft_V	EMIT_20230815T105056	+	+	+	o	+	o	4	+
Budryk_shaft_V	EMIT_20240617T063901	o	o	o	o	+	o	1	-
Budryk_shaft_V	EnMAP_20240920T100233	+	+	+	o	+	o	4	+
Zofiwka_shaft_V	EMIT_20230815T105056	+	+	+	o	+	o	4	+
Zofiwka_shaft_V	EMIT_20240617T063849	+	+	+	o	+	o	4	-
Szczyglowice_shaft_VI	EMIT_20230815T105056	o	+	o	-	+	o	1	-
Szczyglowice_shaft_VI	EMIT_20240617T063849	o	o	o	-	+	o	0	-
Wesola_shaft_A	EMIT_20240617T063901	-	+	o	o	+	o	1	-
Pniówek_shaft_IV	EMIT_20230815T105056	+	+	+	-	+	o	3	+
Pniówek_shaft_IV	EMIT_20240617T063849	o	o	+	-	+	o	1	-
Pniówek_shaft_III	EMIT_20230815T105056	+	o	+	o	+	o	3	-
Pniówek_shaft_III	EMIT_20240617T063849	-	+	+	-	+	o	1	-
Pniówek_shaft_V	EMIT_20230815T105056	+	+	+	o	+	o	4	+
Chwalowice_shaft_V	EMIT_20230815T105056	+	+	+	o	+	o	4	+
Chwalowice_shaft_V	EMIT_20240617T063849	o	o	+	-	+	o	1	-
Chwalowice_shaft_V	EnMAP_20240920T100233	+	+	+	o	+	o	4	-
Sosnica_shaft_V	EMIT_20230815T105056	+	+	+	o	+	o	4	-
Sosnica_shaft_V	EnMAP_20240920T100233	-	+	+	-	+	o	1	-

Table 6: Plume score and its six contributing parameters for all retrieved scenes. The last column gives the score for the suitability for emission estimation. “+” (green) for clearly yes, “-” (red) for clearly no, “o” (blue) for everything in between. The total plume score is the sum (counting + as 1 and – as -1). All scenes with a plume score ≥ 2 are classified as plumes.



<https://eyeclima.eu>

BRUSSELS, 11 03 2025

Funded by the European Union. Views and opinions expressed are however those of the author(s) only and do not necessarily reflect those of the European Union. Neither the European Union nor the granting authority can be held responsible for them.

